Rayleigh-Bénard convection in elliptic and stadium-shaped containers

Worawat Meevasana and Guenter Ahlers
Department of Physics and iQUEST, University of California, Santa Barbara, California 93106
(Received 20 June 2002; published 30 October 2002)

We report on defect formation in convection patterns of stadium-shaped and elliptical horizontal layers of fluid heated from below (Rayleigh-Bénard convection). The fluid was ethanol with a Prandtl number $\sigma = 14.2$. The outermost convection roll was forced to be parallel to the sidewall by a supplementary wall heater. The major- and minor-axis aspect ratios $\Gamma_i = D_i/2d$, $i = 1, 2$ (D_i are the major and minor diameter and d the thickness) were 19.4 and 13.0, respectively. For the stadium shape, we found a stable pattern that was reflection-symmetric about the major diameter and had a downflow roll of length L_s along a large part of this diameter. This roll terminated in two convex disclinations, as expected from theory. No other patterns with the outermost roll parallel to the sidewall were found. The wave numbers of the rolls in the curved sections and L_s decreased with increasing $\epsilon \equiv \Delta T/\Delta T_c - 1$, consistent with a prediction for wave-number selection by curved rolls in an infinite system. At large ϵ, the roll adjacent to the sidewall became unstable due to the cross-roll instability. For the elliptical shape, wave-director frustration yielded a new defect structure predicted by Ercolani *et al*. Depending on the sample history, three different patterns with the outermost roll parallel to the wall were found. For one, the central downflow roll seen in the stadium was shortened to the point where it resembled a single convection cell. Along much of the major diameter there existed an upflow roll. The new defect structure occurred where the two downflow rolls surrounding the central upflow roll joined. This joint, instead of being smooth as in the stadium case, was angular and created a protuberance pointing outward along the major diameter. We also found a pattern with an upflow roll along the major diameter without the central downflow cell. A third pattern contained a downflow cell, but this cell was displaced by a roll width from the center along a minor diameter. As ϵ increased, the length L_e between the two protuberances and the wave numbers along the outer parts of the major diameter decreased for all three patterns, analogous to what was found for the stadium. The upper stability limit of these patterns was also set by the cross-roll instability.

DOI: 10.1103/PhysRevE.66.046308 PACS number(s): 47.54.+r, 47.20.Bp

I. INTRODUCTION

In the absence of significant external noise, ideal two-dimensional patterns in nonlinear dissipative systems can have regular structures with long-range order, such as parallel straight rolls or stripes, squares, or hexagons. Close approximations to this idealization can be found in convection of a thin horizontal layer of fluid heated from below, i.e., in Rayleigh-Bénard convection (RBC) [1]; but the same patterns occur in many other driven systems, including vertically vibrated layers of sand, chemical reactions, and biological systems [2]. An interesting problem is the study of defects that can be induced in such structures. This issue was addressed recently from a mathematical point of view by Ercolani *et al.* [3,4]. The problem is of interest because defects are characteristic of ''natural'' patterns, i.e., of patterns that form in the presence of significant noise and/or boundaries. The defects can be grouped in a small number of universal classes, including domain walls, dislocations, convex and concave disclinations, foci, and spiral defects. In Fig. 1, we show examples of a few of these [5–11].

Here we present the results of an experimental study of a new defect structure which arises as a result of wave-director frustration and which was discussed by Ercolani *et al.* [3,4]. It occurs in samples with elliptical sidewalls when the axis of the outermost roll is forced to be parallel to the wall. When the same is done in a stadium-shaped container (two semicircles connected by a straight section), wave directors emanating from the curved sections of the sidewall will intersect at the centers of the semicircles forming the stadium ends. This is expected to lead to the formation of two convex disclinations connected by a straight roll along the major diameter. However, a similar exercise for an elliptical shape, and indeed for a range of shapes with nonconstant radius of curvature, yields caustics at the points where the wave directors intersect. This is associated with a wave-director frustration that is expected to lead to a new type of defect structure. Here we present shadowgraph images [12] of this structure as well as of convex disclinations which were obtained with RBC samples in elliptical- and stadium-shaped containers, respectively.

For the stadium, we observed the expected convex disclinations, connected by a downflow roll along the major diameter. These structures were stable over the range $0 \lesssim \epsilon \equiv \Delta T/\Delta T_c - 1 \lesssim 2$, and no other patterns were found. As ϵ increased, the wave number of the rolls adjacent to the curved ends decreased, consistent with the known wave-number selection by the curved rolls of foci [13–18]. For ϵ near 2, this wave number became unstable to cross rolls.

For the ellipse, we found that the central downflow roll of the stadium had shrunk so as to form a single downflow cell at the center. Along a significant length of the major diameter there was thus an upflow roll. The adjacent downflow rolls met at an angle, forming two singularities rather than being smoothly curved. At each of the corners, a small protuberance emanated along the major diameter in the direction toward the sidewall. We also found patterns in which the downflow cell at the center was absent, and ones in which a

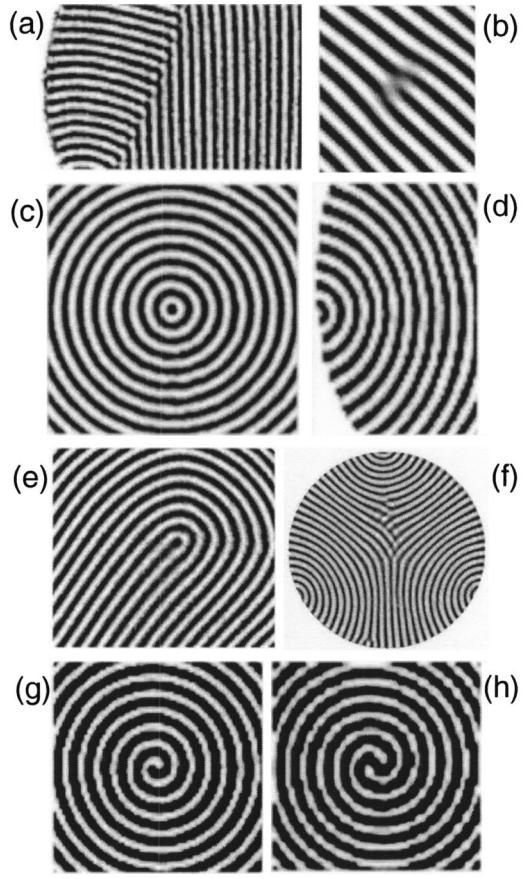

FIG. 1. Shadowgraph images of defects observed in Rayleigh-Bénard convection. Light (dark) areas correspond to downflowing, relatively cold (upflowing, relatively warm) fluid. (a) A domain wall. From Ref. [5]. (b) A dislocation. From Ref. [6]. (c) A focus singularity. From Ref. [7]. (d) A wall focus located at the lateral wall containing the fluid. From Ref. [7]. (e) A convex disclination. From Ref. [8]. (f) A somewhat imperfect concave disclination (three wall foci are also seen). From Ref. [9]. (g) A single-armed spiral defect. From Ref. [10]. (h) A double-armed spiral defect. From Ref. [10].

single upflow cell occurred immersed in the downflow roll adjacent to the major diameter. All three structures were stable over a wide ϵ range. As for the stadium, the distance between the two singularities decreased with increasing ϵ, and at large ϵ the stability limit of these structures was determined by the cross-roll instability. Our results are consistent with the prediction of [3,4].

In the next section, we briefly describe some details of the experiment. In Sec. III A, we present and discuss the patterns that have been found in the stadium-shaped and in the elliptical sample. In Sec. III B, we examine the wave numbers selected by these structures.

II. APPARATUS

We used a standard Rayleigh-Bénard convection apparatus as described elsewhere [19–21]. The cell top was a sapphire, and the bottom was a diamond-machined aluminum plate with a metal-film heater attached to its bottom. The cell wall was made of lexan [22] with a thermal conductivity of 0.23 W/m K. The lexan disk was circular, with a diameter of 9.6 cm. A cell of the desired shape was cut out of its center. Imbedded in the cell wall, parallel and close to the inner cutout, was a second heater consisting of a manganin wire of 0.013 cm diameter with a resistance of approximately 12 Ω. This heater could be used to force convective flow near the wall even slightly below the bulk onset, and could create convection rolls parallel to it. Power dissipation in this heater typically was 1.0 W.

We investigated a stadium-shaped (two semicircles connected by a straight section) and an elliptical cell. For both geometries, the thickness of the cell wall and fluid layer was $d=0.229$ cm. The major (minor) diameter was $D_1=8.89$ ($D_2=5.93$) cm, yielding an aspect ratio $\Gamma_1=D_1/2d=19.4$ ($\Gamma_2=D_2/2d=13.0$). Thus we had $\Gamma_1/\Gamma_2=1.5$. For the stadium, this geometry implies that the length of the straight-walled central section was equal to the radius of the semicircular ends.

We also studied an additional elliptical cell constructed in the same way, except that the thickness of the cell wall and fluid layer was 0.152 cm. This cell had aspect ratios $\Gamma_1=29.1$ and $\Gamma_2=19.5$. For this cell, we were unable to generate patterns that were reflection-symmetric about the major diameter.

The fluid was ethanol at a mean temperature of 32.0 °C with a conductivity of 0.167 W/m K and a Prandtl number $\sigma=14.2$. The vertical thermal diffusion time was $\tau_v=61$ sec. When a temperature difference ΔT was to be applied, the bath (bottom plate) temperature was lowered (raised) by $\Delta T/2$. The critical temperature difference for the onset of convection in the cell with $d=0.229$ cm was $\Delta T_c=1.33$ °C. We estimate $\Delta T_c=4.49$ °C for the cell with $d=0.152$ cm.

Flow visualization was by the shadowgraph method [12]. The images were divided by a reference image and rescaled for optimal visual appearance. Each image was rescaled according to its own standard deviation from its mean. Thus the visual appearance yields no indication of the flow amplitude. In all images, the brightest (darkest) regions correspond to relatively cold downflow (warm upflow).

We used various histories in an attempt to create different patterns in a given cell. It was always easy to create disordered patterns with many roll axes orthogonal to the wall. These were not of interest in the present work. To create the patterns of interest here, we usually kept the power of the wall heater at 1 W and equilibrated the system with no additional power for six hours. In one method we then suddenly set ΔT to 1.6 °C ($\epsilon\simeq 0.2$) and equilibrated for two hours. Thereafter ΔT was increased in steps of 0.2 °C, with equilibration times of 2 h after each step. For the elliptical cell, this usually yielded a pattern with a downflow cell at the geometrical center (see Fig. 3). In the other procedure we equilibrated the system at $\Delta T\simeq 1.0$ °C ($\epsilon\simeq -0.25$) for six hours, followed by a step to $\Delta T=1.6$ °C. This usually yielded patterns like those in Fig. 4 below. For the stadium, these procedures all yielded a single unique pattern. Of course we cannot rule out that other stable patterns can be generated by other procedures. Although considerable time

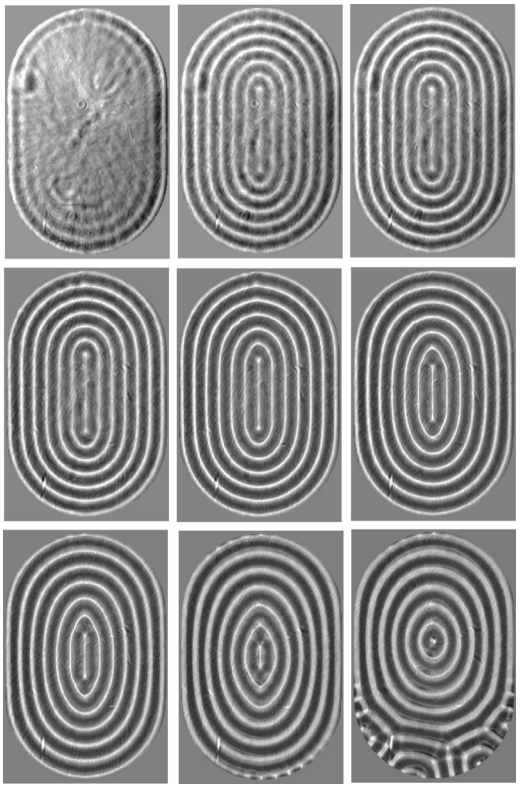

FIG. 2. Patterns obtained in the stadium-shaped cell with $\Gamma_1 = 19.4$ and $\Gamma_2 = 13.0$. From left to right and then top to bottom, the images are for $\epsilon = -0.023$, 0.076, 0.128, 0.203, 0.50, 0.96, 1.26, 1.86, and 2.16.

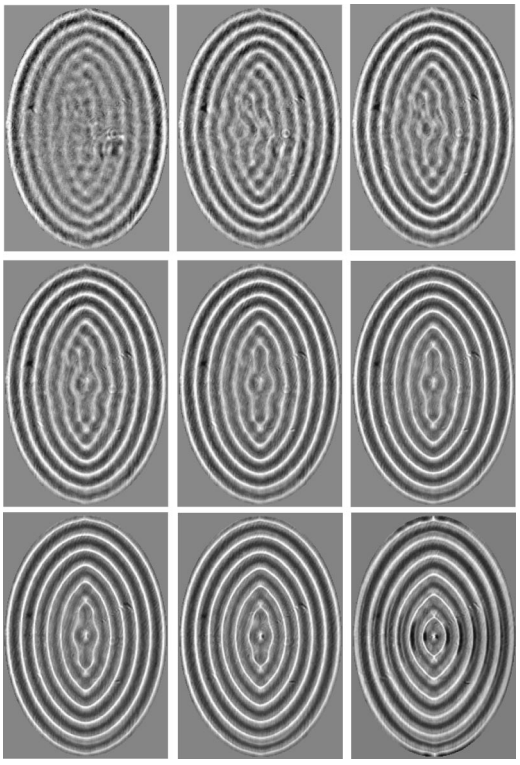

FIG. 3. Symmetric downflow patterns in the elliptical cell with $\Gamma_1 = 19.4$ and $\Gamma_2 = 13.0$. From left to right and then top to bottom, the images are for $\epsilon = -0.023$, 0.076, 0.128, 0.203, 0.35, 0.65, 0.95, 1.26, and 2.01.

was required initially to establish a desired pattern, equilibration to a new wave-number distribution at a new ϵ value was relatively fast and ΔT could be changed at time intervals of one or two hours in increments of 0.1 or 0.2 °C. An image was taken at the end of the equilibration period.

III. RESULTS

A. Patterns

1. Stadium

Patterns obtained in the stadium geometry are shown in Fig. 2 for several values of ϵ. Each contained a straight central roll with downflow along part of the major diameter, terminating in two convex disclinations. The wave numbers of the rolls in the curved section of the pattern decreased with increasing ϵ, with a consequent decrease of the length L of the central roll. At small ϵ, the convex disclinations were essentially perfect. At larger ϵ, the curvature near the disclination of the roll pair surrounding the central roll increased and gave a more angular appearance. The upper stability limit of this pattern type was determined by the cross-roll instability, which caused a breakup of the outermost roll near one curved end of the pattern (see $\epsilon = 1.86$ and 2.16 in Fig. 2). The dependence of L on ϵ will be discussed further below in Sec. III B. At small ϵ, the pattern remained stable until its amplitude vanished for negative ϵ (see the upper left image in Fig. 2).

2. Ellipse

For the ellipse, we were able to generate three different kinds of patterns with the outermost roll parallel to the wall. In all of them there was downflow (bright in the shadowgraph) adjacent to the wall.

Typical examples of the first pattern type are shown in Fig. 3. It had reflection symmetry about the major diameter. A small convection cell with downflow at its center occupied the center of the sample. This cell corresponds to the much longer downflow roll along the major diamater of the stadium; the geometric frustration of the ellipse caused this downflow roll to decrease its length until a stable cell resulted. We will refer to this pattern as a symmetric downflow pattern. Away from the sample center along the major axis there was upflow that terminated in two defects. These defects differ from the convex disclinations encountered in the stadium geometry in that the surrounding downflow region has a protrusion pointing outward along the major diameter. This singularity, called a ''protuberance,'' corresponds to the prediction of Ercolani *et al.* [4] and is the result of the frustration that occurs in the elliptical geometry. Similar patterns have been generated by numerical integration of the Swift-Hohenberg equation [4] and of the Boussinesq equations [23]. The structure is stable over a wide ϵ range.

A second type of pattern had upflow without a central downflow cell along a central part of the major diameter. This upflow roll terminated in two protuberances. The reflection symmetry about the major diameter was broken by the immersion of an upflow cell in the downflow roll adjacent to

the major diameter, as shown in Fig. 4. The upflow cell may be regarded as a bound pair of dislocations of opposite topological charge. We will refer to this pattern as an asymmetric upflow pattern. As seen in the figure, the dislocation pair was stable over a considerable ϵ range, but beyond $\epsilon \simeq 1.6$ it disappeared. This yielded a symmetric upflow pattern at larger ϵ.

In the third pattern (Fig. 5), there is upflow along the central part of the major diameter, and this pattern is reflection-symmetric about the major diameter (symmetric upflow pattern). It is identical to the pattern that evolves from the asymmetric upflow pattern at large $\epsilon \gtrsim 1.6$. The line of upflow again terminates in two protuberances.

A detailed view of the central sections of all four patterns is given in Fig. 6.

The stability ranges of all three patterns for the elliptical sample were similar. Figure 3 illustrates the behavior at small ϵ. As ϵ decreased below about 0.2, some irregularities involving dislocations tended to form near the sample center. At even smaller ϵ, the pattern amplitude vanished in the center while a weak roll system due to the sidewall forcing by the wall heater remained near the wall (see upper left, $\epsilon = -0.02$).

At large ϵ, the patterns became unstable to cross rolls, as can be seen in Fig. 4 for $\epsilon = 2.31$. As the central straight-roll section became shorter, the roll wavelength in the region of greatest curvature increased and locally approached the cross-roll instability [24]. This is similar to what was observed for the stadium (see Fig. 2 at $\epsilon = 1.86$ and 2.16), but for the ellipse the instability occurred at a slightly larger ϵ value.

We also attempted to establish patterns of high symmetry in an elliptical cell with larger aspect ratios [25] ($\Gamma_1 = 29.1$ and $\Gamma_2 = 19.5$), but were not very successful. In Fig. 7, we show some of our results. Each pattern was equilibrated for six hours before the image was taken. The patterns were not reflection-symmetric about their major diameter. They became unstable to cross rolls near the wall in the area of

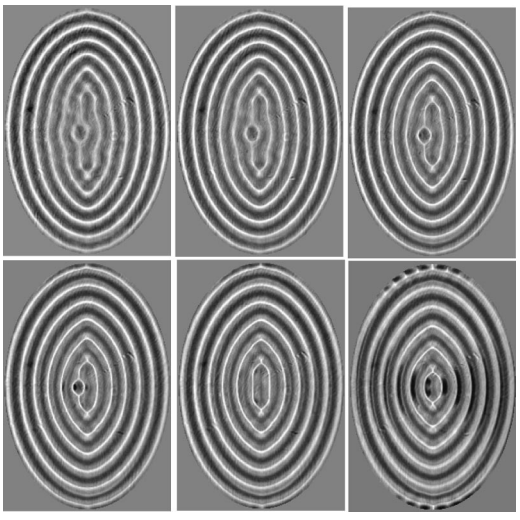

FIG. 4. Asymmetric upflow patterns in the elliptical cell with $\Gamma_1 = 19.4$ and $\Gamma_2 = 13.0$. From left to right and then top to bottom, the images are for $\epsilon = 0.35$, 0.65, 1.10, 1.56, 1.71, and 2.31.

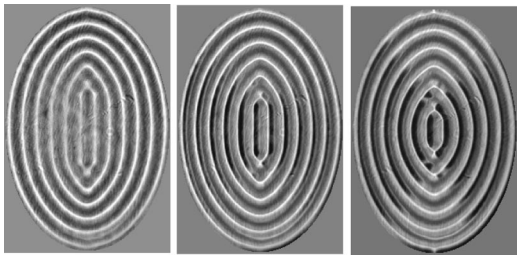

FIG. 5. Symmetric upflow patterns in the elliptical cell with $\Gamma_1 = 19.4$ and $\Gamma_2 = 13.0$. From left to right, the images are for $\epsilon = 0.35$, 1.10, and 1.86.

largest curvature already for $\epsilon \simeq 0.4$, which is much smaller than the stability limit for the smaller-Γ cell. In Fig. 8, we show the central section of the pattern for $\epsilon = 0.11$. Although the pattern contains a variety of defects, some of these do have similarities to the defects in reflection-symmetric patterns generated by Ercolani *et al.* [4] by numerical integration of the Swift-Hohenberg equation.

B. Wave numbers

At modest or large ϵ, the smallest wavelengths (largest wave vectors) of the patterns are along the minor diameter. In this direction, the phase of the pattern is pinned at the two opposite walls, and thus the number of rolls and average wavelength $\overline{\lambda}_{2,i}, i = s, e$ are independent of ϵ. For the stadium patterns (s) and for the symmetric upflow patterns of the ellipse (e) there were $N_{2,s} = 12$ and $N_{2,e} = 11$ roll pairs,

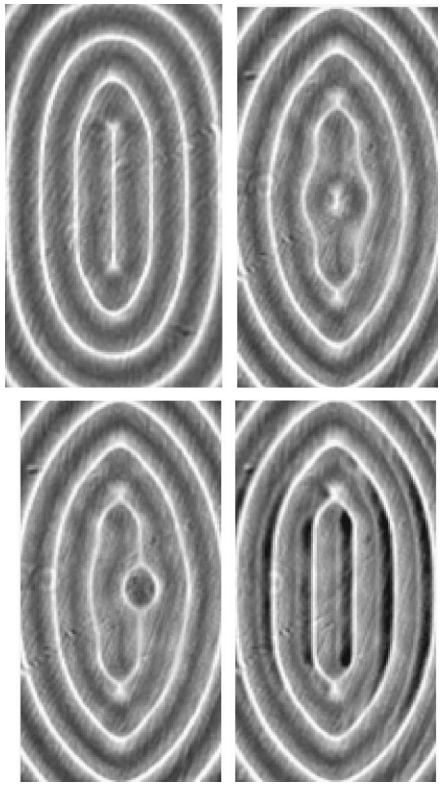

FIG. 6. Detailed views of the central sections of the stadium pattern (top left) and the three elliptical patterns for $\epsilon = 0.95$.

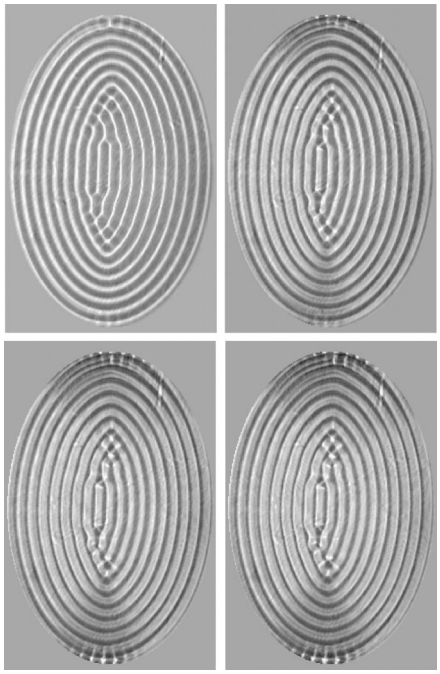

FIG. 7. Patterns obtained in a cell with $\Gamma_1=29.1$ and $\Gamma_2=19.5$. From left to right and then top to bottom the images are for $\epsilon=0.11$, 0.29, 0.38, and 0.42. The last pattern, at $\epsilon=0.42$, was unstable and over many hours evolved to a pattern with roll axes orthogonal to the sidewall.

respectively, along the minor diameter. In units of the cell spacing d, this corresponds to $\overline{\lambda}_{2,i}=2\Gamma_2/N_{2,i}=2.17$ and 2.36, respectively. The corresponding average wave vectors $\overline{k}_{2,i}=2\pi/\overline{\lambda}_{2,i}$ are 2.90 and 2.66, respectively, somewhat smaller than the critical wave vector $k_c=3.117$ at onset of convection. For the symmetric downflow pattern of the ellipse, $\overline{\lambda}_{2,e}$ and $\overline{k}_{2,e}$ are the same as for the stadium patterns.

Along the major diameter, the phase of the rolls is also pinned at the walls, but it is free at the disclinations or protuberances because the central roll can adjust its length. This provides the opportunity for a wave-number selection process to become effective and the wavelengths and numbers $\overline{\lambda}_{1,i}$ and $\overline{k}_{1,i}$ in this direction can depend on ϵ. The length L_s of the downflow roll along the major diameter of the stadium is shown as open circles in Fig. 9. Also shown are the distances L_e between the extreme ends of the protuberances of the symmetric downflow (solid circles), symmetric upflow (crosses), and asymmetric upflow (pluses) patterns, respectively. One sees that L_e is the same within our resolution for the three elliptical patterns, but that it is somewhat larger

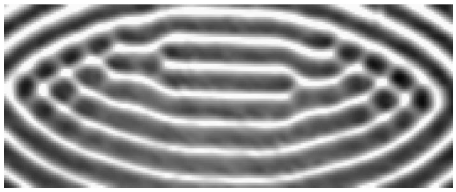

FIG. 8. A detailed view of the pattern for $\Gamma_1=29.1$, $\Gamma_2=19.5$, and $\epsilon=0.11$.

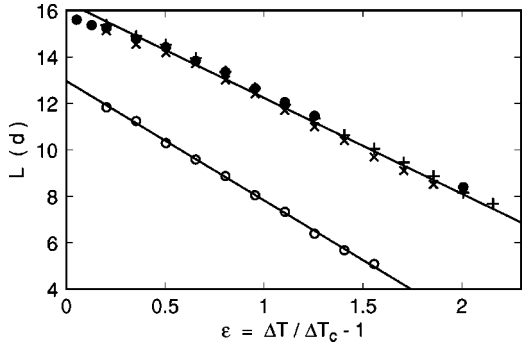

FIG. 9. The lengths L_s and L_e of the central straight sections of the patterns. The open circles are for the stadium (L_s). The remaining data are for the symmetric downflow patterns (solid circles), symmetric upflow patterns (crosses), and asymmetric upflow patterns (pluses) of the ellipse (L_e). The solid lines represent fits of Eq. (1) separately to the stadium and the ellipse results.

than L_s for the stadium. Except perhaps for very small ϵ, we can represent $L_i, i=s,e$ by a straight line,

$$L_i=A_i+B_i\epsilon, \tag{1}$$

as shown by the two solid lines in the figure. With L_i in units of d, we find $A_s=12.96$, $B_s=-5.14$, $A_e=16.36$, and $B_e=-4.12$.

For all three elliptical patterns, there are $N_e=5$ roll pairs between the protuberance and the cell wall. For the stadium, however, there are $N_s=6$ roll pairs between the disclination

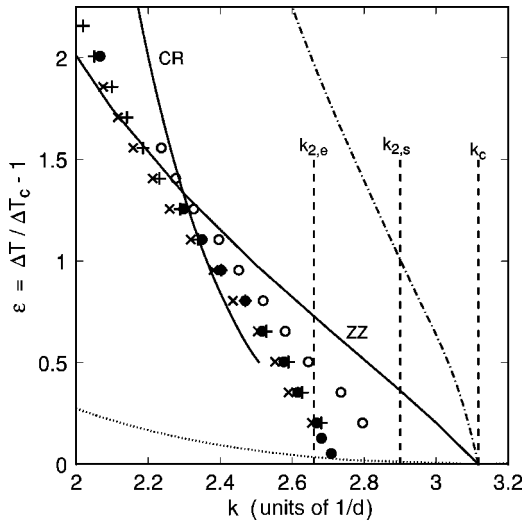

FIG. 10. The average wave number $\overline{k}_{1,i}, i=s,e$ along the major diameter between the disclination/protuberance and the sidewall. The open circles are for the stadium. The remaining data are for the symmetric downflow patterns (solid circles), symmetric upflow patterns (crosses), and asymmetric upflow patterns (pluses) of the ellipse. The dotted line is the neutral curve of the infinite system. The two solid lines are the zig-zag instability (ZZ) and the cross-roll instability (CR) of the infinite system of parallel straight rolls and $\sigma=14.2$. The three vertical dashed lines correspond to the wave numbers $\overline{k}_{2,i}$ along the minor diameter and to k_c. The dash-dotted line is the theoretical result [18] for the wave number selected by the focus singularity of the axisymmetric pattern and for $\sigma=7$.

and the wall. The average wave number of the rolls between the disclination/protuberance and the wall is given by $\overline{k}_{1,i} = 2\pi/[(\Gamma_1 - L_i/2)/N_i]$. Results for $k_{1,i}$ are shown in Fig. 10. At small ϵ, the selected $\overline{k}_{1,i}$ depends on the geometry, but for both cases it is considerably smaller than the critical wave number k_c (the $\overline{k}_{2,i}$ and k_c are shown as dashed vertical lines in the figure). For small ϵ, the values of $\overline{k}_{1,i}$ lie below the zig-zag bulk instability line [24,26] of the laterally infinite uniform roll system. Presumably the roll curvature and finite system size stabilize the rolls in spite of the known bulk instability [27–30]. At modest and large ϵ, one sees that the ellipse and the stadium select very similar average wave numbers along the major diameter. At large ϵ, the values of $\overline{k}_{1,i}$ lie well to the left of the cross-roll instability [24,26] of the bulk system. Again one concludes that the finite system size and/or roll curvature provide stabilization. In this case, the experimentally observed stability limit of the finite pattern to cross rolls (see Figs. 2 and 4) occurs at wave numbers that are significantly smaller than the stability limit of the infinite system.

Finally, we compare the selected wave numbers $\overline{k}_{1,i}$ with the prediction by Buell and Catton [18,26] of the wave number selected by axisymmetric convection (focus patterns), which is given by the dash-dotted line in Fig. 10. This line, being for the infinitely extended system, must of course start at k_c and $\epsilon = 0$ and thus cannot agree with the experiments for the finite system. We see, however, that the prediction and the data are nearly parallel to each other, suggesting that the selection by roll curvature in our physical system is closely related to the mechanism treated in the theory for the infinite system.

ACKNOWLEDGMENTS

We are grateful to Kapil Bajaj for his assistance and guidance during the early stages of this project, and to Nicholas Ercolani for calling our attention to this interesting problem. We wish to thank Werner Pesch for permitting us to use his program for the calculation of the ZZ and the CR instability lines in Fig. 10. This work was supported through Department of Energy Grant No. DE-FG0387.

[1] For a review, see, for instance, E. Bodenschatz, W. Pesch, and G. Ahlers, Annu. Rev. Fluid Mech. **32**, 709 (2000).
[2] For a review, see M.C. Cross and P.C. Hohenberg, Rev. Mod. Phys. **65**, 851 (1993).
[3] N.M. Ercolani, R. Indik, A.C. Newell, and T. Passot, J. Nonlinear Sci. **10**, 223 (2000).
[4] N. M. Ercolani, R. Indik, A. C. Newell, and T. Passot, Physica D (to be published).
[5] Y. Hu, R.E. Ecke, and G. Ahlers, Phys. Rev. E **55**, 6928 (1997).
[6] K. M. S. Bajaj, N. Mukolobwiez, and G. Ahlers (unpublished).
[7] Y. Hu, R.E. Ecke, and G. Ahlers, Phys. Rev. E **48**, 4399 (1993).
[8] J. Liu and G. Ahlers, Phys. Rev. E **55**, 6950 (1997).
[9] J. Liu and G. Ahlers, Phys. Rev. Lett. **77**, 3126 (1996).
[10] E. Bodenschatz, J.R. de Bruyn, G. Ahlers, and D.S. Cannell, Phys. Rev. Lett. **67**, 3078 (1991).
[11] Examples of patterns from Rayleigh-Bénard convection, including the ones in Fig. 1, can be found at http://www.nls.physics.ucsb.edu by following the link ''picture page.''
[12] J.R. deBruyn, E. Bodenschatz, S. Morris, S. Trainoff, Y.-C. Hu, D.S. Cannell, and G. Ahlers, Rev. Sci. Instrum. **67**, 2043 (1996).
[13] L. Koschmieder and S. G. Pallas, Int. J. Heat Mass Trans. **17**, 991 (1974); L. Koschmieder, Adv. Chem. Phys. **26**, 177 (1974).
[14] V. Croquette and A. Pocheau, in *Cellular Structures in Instabilities*, edited by J. E. Wesfreid and S. Zaleski (Springer, Berlin, 1984), p. 104.
[15] V. Steinberg, G. Ahlers, and D.S. Cannell, Phys. Scr., T **T9**, 97 (1985); Phys. Scr. **32**, 534 (1985).
[16] P. Manneville and J.M. Piquemal, Phys. Rev. A **28**, 1774 (1983).
[17] M.C. Cross, Phys. Rev. A **27**, 490 (1983).
[18] J.C. Buell and I. Catton, Phys. Fluids **29**, 23 (1986).
[19] L.I. Berge, G. Ahlers, and D.S. Cannell, Phys. Rev. E **48**, R3236 (1994).
[20] G. Ahlers, L.I. Berge, and D.S. Cannell, Phys. Rev. Lett. **70**, 2399 (1993).
[21] G. Ahlers, D.S. Cannell, L.I. Berge, and S. Sakurai, Phys. Rev. E **49**, 545 (1994).
[22] Lexan is a polycarbonate plastic.
[23] M. Paul (private communication).
[24] F.H. Busse and R.M. Clever, J. Fluid Mech. **91**, 319 (1979).
[25] In an attempt to stabilize the roll parallel to the sidewall, we increased the power of the wall heater to 2.6 W.
[26] The theoretical results from Refs. [24] and [18] are for $\sigma = 7$. The zig-zag and cross-roll instabilities for our $\sigma = 14.2$ were calculated using a program provided by W. Pesch. The curvature-selected wave number is not expected to be very sensitive to σ [18].
[27] For one-dimensional structures, and particularly for Taylor-vortex flow, it has long been known that the bulk instability (the Eckhaus instability in this case) is suppressed [28–30]. The instability line meets the neutral curve below and above k_c, thus opening a gap in which the structure is stable until its amplitude vanishes on the neutral curve.
[28] L. Kramer and W. Zimmermann, Physica D **16**, 221 (1985).
[29] R. Heinrichs, G. Ahlers, and D.S. Cannell, Phys. Rev. Lett. **56**, 1794 (1986).
[30] G. Ahlers, D.S. Cannell, M.A. Dominguez-Lerma, and R. Heinrichs, Physica D **23**, 202 (1986).